JOURNAL OF CHEMICAL INFORMATION AND MODELING

Article

pubs.acs.org/jcim

Interactions and Stabilities of the UV RESISTANCE LOCUS8 (UVR8) Protein Dimer and Its Key Mutants

Min Wu,[†] Åke Strid,[‡] and Leif A. Eriksson*[,†]

[†]Department of Chemistry and Molecular Biology, University of Gothenburg, SE-412 96 Göteborg, Sweden

[‡]School of Science and Technology, Örebro University, SE-70182 Örebro, Sweden

Supporting Information

ABSTRACT: The dimeric UVR8 protein is an ultraviolet-B radiation (280−315 nm) photoreceptor responsible for the first step in UV−B regulation of gene expression in plants. Its action comprises the actual absorption of the UV quanta by a tryptophan array at the protein−protein interface, followed by monomerization and subsequent aggregation with downstream signaling components. A crystal structure of the *Arabidopsis thaliana* tryptophan-rich wild type UVR8 protein dimer was recently published, showing the presence of several salt bridges involving arginines R146, R286, R338, and R354. In this work, molecular dynamics simulations in conjunction with umbrella sampling were used to calculate the binding free energy for the wild type UVR8 dimer and three of its mutants (R286A, R338A, and R286A/R338A), in order to verify whether the key mutants are able to disrupt the dimeric structure as indicated experimentally.

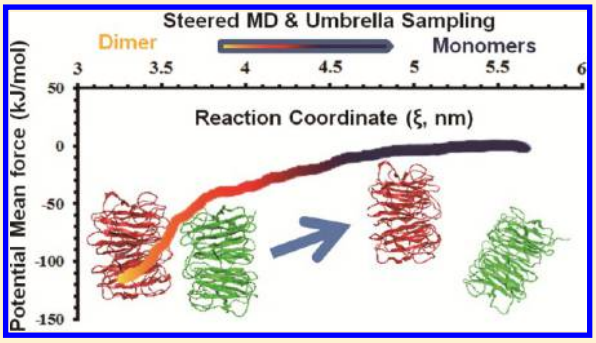

1. INTRODUCTION

UV−B radiation (UV−B; 280−315 nm) is part of the solar spectrum that reaches the surface of the earth. It affects biological molecules and therefore also cells and living organisms, including plants.[1,2] Plant responses include molecular and intracellular changes such as induction of UV−B-responsive genes,[3] photolysis of pyridoxine (vitamin B_6),[4] accumulation of flavonoid-derived pigments, induction of antioxidant systems and DNA repair enzymes,[3] as well as altered plant morphology resulting in decreased leaf size, increased leaf thickness, increased branching, and deposition of wax on the upper cuticle of leaves.[5]

The *Arabidopsis thaliana* UV RESISTANCE LOCUS8 (UVR8) protein has been identified to specifically mediate photomorphogenic UV−B responses by acting as a UV−B photoreceptor.[6−10] UVR8 is involved in orchestrating the expression of more than 100 genes[6,9,11,12] and is suggested to have appeared early in the evolution of plants, in order for them to survive exposure to the UV−B fraction of sunlight.[13,14] An action spectrum of UVR8 function indicates that UVR8 is most effective at 280 nm with the critical action at 290 nm and 300 nm. Since 280 nm rarely reaches the surface of the earth, the longer wavelengths (290 nm and 300 nm) are the most physiologically relevant.[15] The UVR8 protein is a dimer located in the cellular cytosol, and dissociates into a signaling-active monomer upon UV−B exposure.[14]

The 3D structure of the wild type UVR8 core domain, which has recently been published, shows the dimer structure with a seven-bladed propeller WD40 repeat domain in each monomer.[7,10] However, the 11 most N-terminal amino acids and the 55 C-terminal amino acids are missing from the crystal structure. Although the N-terminal 23 amino acids have been identified to play a key role in the nuclear import mechanism,[13] the N-terminal deletion protein is still capable of binding to chromatin at the bZIP transcription factor Elongated hypocotyl5 (HY5) promoter, similarly to the wild type UVR8. Twenty-seven amino acids (aa. 397−423) located at the C-terminus are demonstrated to be necessary and sufficient for the interaction with the seven-bladed WD40 propeller domain of CONSTITUTIVELY PHOTOMORPHOGENIC 1 (COP1),[16] which is known as a repressor of photomorphogenesis in darkness but also as a positive regulator of UV−B-specific responses.[17,18] *A. thaliana* UVR8 has 14 tryptophan residues that are highly conserved among plant species.[7,14,19] The positions of 13 of the tryptophans are present in the crystal structure,[7,10] whereas residue W400 is located in the missing C-terminus region. Residues W39, W196, W300, and W92 were identified to take part in the maintenance of the WD40 structure by hydrogen bonds and hydrophobic interactions,[20] and residues W94, W198, W233, W250, W285, W302, and W337 are positionally located in the dimeric interface. Both dimer and monomer structures are observed in the absence of UV−B after W233A and W337A mutations. W285A and W39A mutants, on the other hand, are constitutive monomers, and W233F and W285F mutants are constitutive dimers both in the absence and in the presence of UV−B. It was shown that residue W285 plays a critical role both in the dimerization of UVR8 monomers and in UV−B perception, and residue W233 plays an essential role in UV−B perception.[7,10,14,20]

Received: March 27, 2013
Published: June 9, 2013

dx.doi.org/10.1021/ci4001822 | *J. Chem. Inf. Model.* 2013, 53, 1736−1746

Several salt bridges involving arginines R146, R286, R338, and R354 were found in the crystal structure,[7,10] but the crystal data are not unambiguous. In one study, the UVR8^{R286A} mutant protein was shown to retain the dimeric structure and undergo UV−B-induced monomerization, whereas the dimeric structure was disrupted entirely by the double mutation R286A/R338A, when assayed by size exclusion chromatography.[7] However, in another paper, the UVR8^{R286A} mutant protein was demonstrated to be monomeric already in the absence of UV−B, when investigated by gel filtration.[10]

In order to investigate the strengths of the monomer−monomer interactions in the wild type UVR8 dimer and its mutants R286A and R286A/R338A and the influence by the single mutant R338A, the free energy (ΔG) of dissociation of the wild type UVR8 dimer and its mutants R286A, R338A, and R286A/R338A were calculated in this work using molecular dynamics (MD), steered molecular dynamics (SMD), and umbrella sampling simulations with the weighted histogram analysis method (WHAM).[21−24] This is a common method to extract equilibrium data from the nonequilibrium SMD trajectories for the calculation of ΔG and enables a direct and quantitative comparison between systems. MD simulation is a useful method in studying interactions between proteins, lipids, nanotubes, and small molecules and provides atomic-level detail of many phenomena. However, it is sometimes not possible to obtain the behavior of systems toward a particular phenomenon due to the time scales involved, e.g. protein−protein interaction, protein−ligand binding, and the motion of drug molecules in lipid bilayers.[25] In such cases, SMD simulations are employed to investigate various processes. With the umbrella-sampling method, we can generate ensemble configurations along a reaction coordinate ξ between two interacting species. Within each configuration, the potential mean force (PMF) is calculated using the WHAM method.[21−24] Energy values are then obtained through PMF curves as a function of the reaction coordinate ξ.[26−28] These have been successfully used to compute the binding free energy for many systems.[29−31] In this work, the binding free energy differences of mutants relative to the wild type UVR8 dimer were calculated.

2. METHODOLOGY

The structure of the UVR8 dimer determined using X-ray diffraction (PDB code: 4DNW[10]) was chosen as a starting model for this work. Each monomer comprises residues 12−385, i.e., lacking the N- and C-terminal tails. The three mutants investigated in this work are the single mutants R286A and R338A and the double mutant R286A/R338A. The mutations of R286 and R338 to alanine were used to alter the contribution of the salt bridges present at the interface between the UVR8 monomers to destabilize the dimer structure by removing favorable electrostatic and hydrogen bonding interactions. In each case, the mutations were introduced on both monomers.

All titratable amino acids in the wild type UVR8 dimer were assigned their canonical protonation state by the 3Dprotonate-algorithm in MOE 2011.[32] The molecular simulations were carried out with the Gromacs 4.5.5 package.[33,34] The Amber03 force field[35] was employed for all MD simulations and energy minimizations in this work. For short-range nonbonded interactions, a cutoff of 1.4 nm was used, with long-range electrostatic interactions calculated using the particle mesh Ewald (PME) algorithm.[36,37] Dispersion corrections were applied to the energy and pressure terms to account for the truncation of the van der Waals terms, and periodic boundary conditions were applied in all directions.

In order to generate equilibrated starting structures for the pulling (SMD) simulations, the mutant structures were generated using the crystal structure of the wild type UVR8 dimer, solvated by TIP3P water molecules, and Na^+ counterions were added as required to neutralize the total charge of the systems. Following steepest descents minimization, each system was equilibrated with position restraints applied to peptide heavy atoms for 100 ps under a constant volume (NVT) ensemble, with protein and nonprotein atoms coupled to separate constant temperature thermostats (310 K) using the Berendsen weak coupling method.[38] This was followed by 100 ps of constant pressure (NPT) equilibration, using a weak coupling to maintain the pressure isotropically at 1.0 bar. The final MD simulations were performed for 100 ns with the NPT ensemble in the absence of any restraints. For this data collection period, the Nosé−Hoover thermostat[39,40] was used to maintain temperature, and the Parrinello−Rahman barostat[41,42] was used to isotropically regulate pressure.

The structures taken at the end of each trajectory (WT, R286A, R338A, and R286A/R338A) were used as starting points for the pulling simulations. They were placed in a rectangular box with dimensions 8 × 20 × 8 nm; sufficient to satisfy the minimum image convention and provide space for pulling simulations to take place along the y axis (cf. Figure 1A). As before, the structures were solvated with TIP3P water molecules, and Na^+ counterions were added as required to neutralize the total charge of the systems. Equilibration was performed for 500 ps using an NPT ensemble, using the same methodology as described before, with position restraints applied to the peptide heavy atoms.

Following equilibration, restraints were removed from monomer B (Figure 1A), and monomer A was used as an immobile reference for the pulling simulations. For each of the systems, monomer B was pulled away from the core structure along the y axis for over 5000 ps, using a spring constant of 1000 kJ/mol/nm^2 and a pull rate of 0.001 nm/ps. The final center of mass (COM) distance between monomers A and B was approximately 5.5 nm. From these trajectories, 14−16 snapshots were taken to generate starting configurations for umbrella sampling windows.[26−28] An asymmetric distribution of sampling windows was used, with a window spacing of 0.05 nm up to 3.5 nm COM separation and of 0.2 nm beyond 3.5 nm COM separation. This allows for increasing detail at smaller COM distances and resulted in 14−16 windows for each system in order to ensure the resulting histograms show continuous overlap, cf., Supporting Information Figure S1. In each window, 40 ns MD simulation was performed, giving a total simulation time of 560−640 ns for umbrella sampling of each system, leading to asymptotic behavior of ΔG_{Bind} as a function of simulation time. The difference of ΔG_{Bind} was less than 0.3 kJ/mol after 35 ns simulation time, as seen in Supporting Information Figure S2. Analysis of the results was performed with WHAM.[21−24] Each system has around 10 000 protein atoms with approximately 25 000 solvent molecules in the MD simulations and ∼40 000 solvent molecules in the SMD and umbrella sampling simulations.

3. RESULTS AND DISCUSSION

Although the 11 N-terminal residues are missing in the 3D structure,[10] all amino acids are, in this paper, referred to by their position in the full length UVR8.

3.1. Structural Details of Mutant Systems from MD Simulations. Images of the starting structures (wild type and mutants) used in pulling simulations are shown in Figure 1B and

dx.doi.org/10.1021/ci4001822 | J. Chem. Inf. Model. 2013, 53, 1736−1746

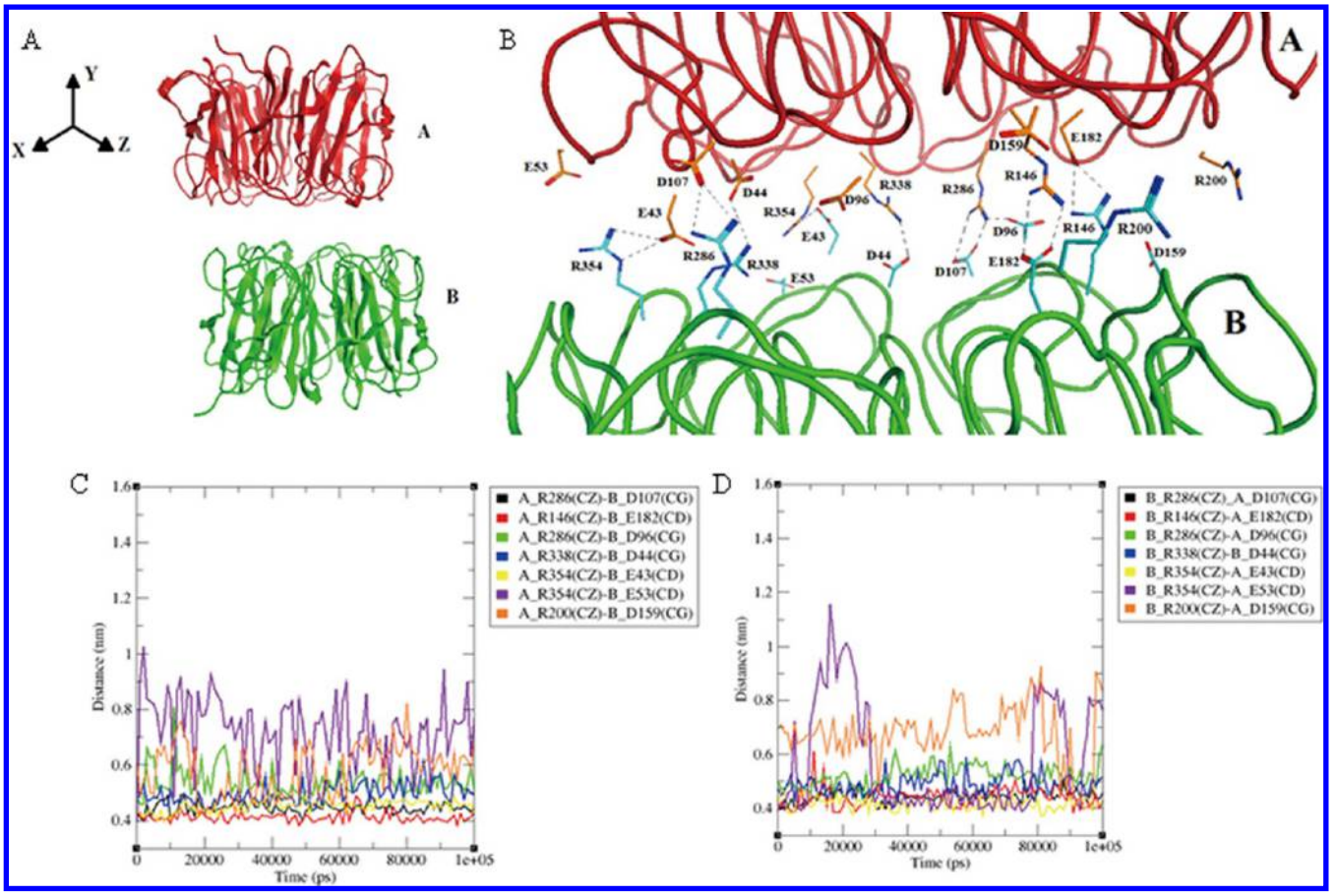

Figure 1. (A) X-ray structure of the UVR8 dimer (PDB code: 4DNW) with each monomer labeled according to the nomenclature used in this paper. Axes are shown to illustrate the pulling direction (the *y* direction). (B) The wild type UVR8 dimer structure; the ribbons of monomer A colored red and monomer B colored green. The amino acid salt bridges involved in monomer A are colored orange, and in monomer B blue. Backbones are not displayed. (C) The distances between CZs (arginine) in monomer A and atom type CDs (glutamic acid)/CGs (aspartic acid) in monomer B in the wild type UVR8 dimer. (D) The distances between CZs (arginine) in monomer B and atom type CDs (glutamic acid)/CGs (aspartic acid) in monomer A in the wild type UVR8 dimer. Atom types CZ and CD/CG represent the carbons from the guanidine group of arginine and the carboxylate group of glutamic acid/aspartic acid, respectively, as defined in the Supporting Information Figure S3.

in the Supporting Information Figure S4. These structures were taken after 100 ns of unrestrained MD simulations. Alpha-carbon root mean square deviation (Cα-RMSD) values and differences in average solvent accessible surface areas (SASA) for each system are listed in Table 1. The values represent averages calculated over the last 30 ns of the simulations.

Table 1. Cα-RMSD Values after 100 ns of MD Simulations

system	[a]Cα RMSD ± std dev (nm)	[b]ΔSASA (nm^2)
wild type	0.1589 ± 0.029	
R286A	0.1542 ± 0.013	4.05
R338A	0.1703 ± 0.029	6.89
R286A/R338A	0.2264 ± 0.025	10.29

[a]Average Cα RMSD value with fluctuation (±SD) of each system during the last 30 ns of the simulations compared to their corresponding starting structures. [b]Relative average solvent accessible surface area (SASA) for each mutant protein in the last 30 ns of the simulations, compared to the wild type UVR8.

In the crystal structure, the acidic (aspartic acid/glutamic acid) and basic (lysine/arginine) surface patches from one UVR8 monomer interact with the other UVR8 monomer's basic and acidic surface patches, respectively, by intermonomeric hydrogen bonds to form a symmetric homodimer. The distances for the formed salt bridges were measured between atom type CZ, representing the central carbons from the guanidinium groups of arginines, and atom type CD/CG representing carbons from the carboxylate groups of glutamic acids/aspartic acids of the respective monomers at the interface. The distances between R146(CZ)−E182(CD) and R286(CZ)−D107(CG) are approximately 0.4 nm, and the amino acid residues form double hydrogen-bonded salt bridges between each other. The distances for single hydrogen-bonded salt bridges are around 0.49 nm for R286(CZ)−D96(CG) and R338(CZ)−D44(CG) and 0.44 nm for R354(CZ)−E43/E53(CD). In the 100 ns simulations, the interface of the wild type UVR8 dimer shows a maintained integrity of the hydrophobic core. The average Cα-RMSD value from the last 30 ns of the simulations is 0.159 nm. The distances between R286(CZ) and D107(CG) and between R146(CZ) and E182(CD) are relatively stable, cf. Figure 1C,D. This shows that the salt bridges contributed by these residues are conserved along the simulations. The distances for the salt bridges R354(CZ)−E43(CD) are approximately 0.43 nm and display small fluctuations, whereas the distances observed for salt bridges R354(CZ)−E53(CD) fluctuate dramatically. This is indicative of weak salt bridge interactions between residue R354 and E53, and they are disrupted in the last snapshot of the MD simulations, cf.

dx.doi.org/10.1021/ci4001822 | J. Chem. Inf. Model. 2013, 53, 1736−1746

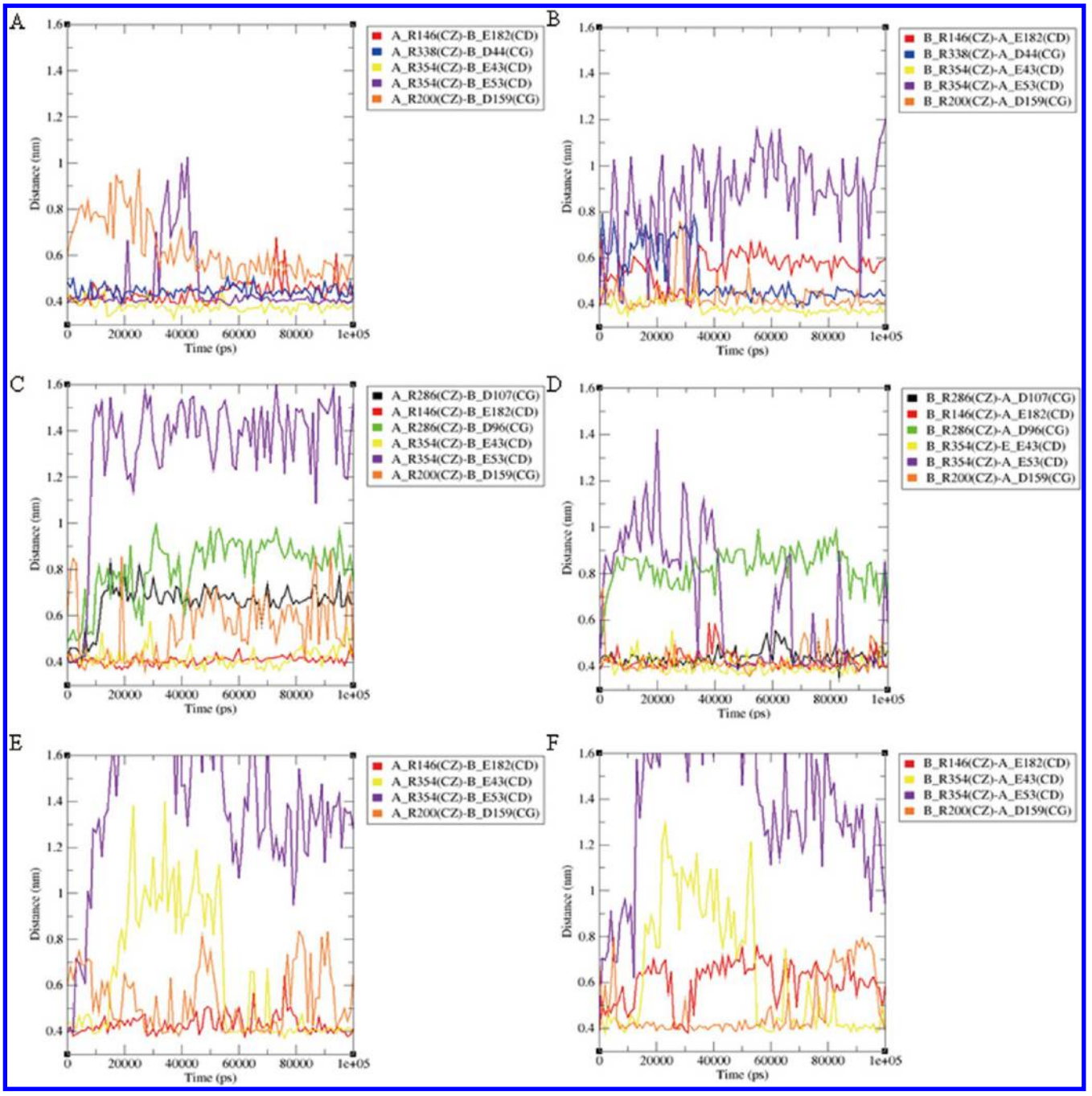

Figure 2. (A) The distances between CZs (arginine) in monomer A and atom type CDs (glutamic acid)/CGs (aspartic acid) in monomer B in the R286A mutant. (B) The distances between CZs (arginine) in monomer B and atom type CDs (glutamic acid)/CGs (aspartic acid) in monomer A in the R286A mutant. (C) Same as for A but in the R338A mutant. (D) Same as for B but in the R338 mutant. (E) Same as for A but in the R286A/R338A double mutant. (F) Same as for B but in the R286A/R338A double mutant. Atom types CZ and CD/CG represent the carbons from the guanidinium group of arginine and the carboxylate group of glutamic acid/aspartic acid, as defined in the Supporting Information Figure S3.

Figure 1B. The distances between the carbons of the guanidinium groups of R200 and the carboxylate groups of D159 are approximately 0.68 nm in the crystal structure and fluctuate dramatically along the MD simulations, similar to the salt bridge R354−E53. Due to their close spatial location, a weak salt bridge is thus formed and interrupted throughout the MD simulation,

For UVR8 containing mutation R286A, the average Cα-RMSD value is 0.154 nm in the last 30 ns of the simulations, similar to the wild type UVR8 dimer. The double hydrogen-bonded salt bridges between R286 and D107 and the single hydrogen-bonded salt bridges linking R354 in monomer B with E53 in part A and R286 with D96 are missing. From Figure 2 A,B, it can be seen that the distance fluctuations between related salt bridge residues are not equal in the two monomers. R146, R338, and R354 residues in monomer A strongly interact with E182, D44, and E43 in monomer B, respectively, as seen from their small fluctuations in distances. The distance between R338(CZ) in monomer B and D44(CG) in monomer A, on the other hand, fluctuates dramatically after the R286A mutation and reaches a stable distance after 35 ns. The long distance of approximately ~0.55 nm between R146(CZ) in monomer B and E182(CD) in monomer A during the last 60 ns indicates a very weak

dx.doi.org/10.1021/ci4001822 | J. Chem. Inf. Model. 2013, 53, 1736−1746

interaction compared to its R146^{A}–E182^{B} counterpart. The distance between R354(CZ) in monomer A and E53(CD) in monomer B fluctuates only slightly along the simulation, expect during the interval 30–42 ns. Its corresponding R354^{B}–E53^{A} counterpart, on the other hand, displays large fluctuations (0.4–1.2 nm) throughout the simulation. During the last 30 MD simulations, the distance between R200(CZ) and D159(CG) is reduced to becoming relatively short and stable, resulting in the occurrence of the salt bridges displayed in the last snapshot, as shown in Supporting Information Figure S4.

Mutation of R338 to alanine results in a relatively large average Cα-RMSD value of ~0.170 nm from the last 30 ns of the simulations compared to the wild type UVR8 dimer. The double hydrogen-bonded salt bridge between R286 in monomer A and D107 in monomer B, and single hydrogen-bonded salt bridges R286–D96, R338–D44, and R345–E53 are interrupted in the last snapshot (shown in Supporting Information Figure S4). The distances between R146(CZ) and E182(CD) and between R354(CZ) and E43(CG) are around 0.43 nm with small fluctuations along the MD simulations, cf. Figure 2C,D, leading to conservation of the single hydrogen-bonded salt bridge R354–E43 and double hydrogen-bonded E182–R146 salt bridge as displayed in the last snapshot. R200–D159 salt bridges are also formed in the last snapshot structure. However, the distances between R200(CZ) in monomer B and D159(CG) in monomer A are shorter and overall display much smaller fluctuations than R200(CZ) in monomer A and D159(CG) in monomer B. Again, the behavior of the corresponding interaction sites of the monomers is thus not identical.

The double mutation of UVR8 residues R286 and R338 to alanines leads to a partly dissociated structure, with a large average Cα-RMSD value (~0.226 nm from the last 30 ns simulations). In this case, the average distance between R146(CZ) in monomer A and E182(CD) is 0.43 nm with a small fluctuation during the simulation, leading to a conserved double hydrogen-bonded salt bridge in the last snapshot (Supporting Information Figure S4). The distance between R354 and E43 is increased after 20 ns and reduced to 0.42 nm with relatively small fluctuations in the last 20 ns, as shown in Figure 2 E,F, whereas the R354–E53 salt bridges are disrupted during the simulations. The distances between R200(CZ) in monomer A and D159(CG) in monomer B fluctuate dramatically, leading to a weak salt bridge interaction between these residues, whereas a strong salt bridge interaction between R200(CZ) in monomer B and D159(CG) in monomer A is noted at 10–70 ns, whereafter it is interrupted.

Mutations at the interface of the UVR8 dimer leads to an increased solvent accessible surface area (SASA) over the course of the 100 ns MD trajectories, although parts A and B do not completely dissociate from the core of the structure in any of the systems. The increased solvation of the dimer interface does, however, lead to destabilization of the dimer structures. In order to quantify this observation, the average SASAs of each system from the last 30 ns simulations were calculated using the YASARA software[43] (listed in Table 1). Compared to the structure of the wild type UVR8 dimer, the average SASA of the R286A mutant structure during the last 30 ns of the simulation is increased by approximately 4.05 nm^2. In the case of the single mutant R338A and the double mutant R286A/R338A structures, the average SASAs are increased by about 6.89 and 10.29 nm^2, respectively. The increased SASAs correlate well with the disrupted salt bridges discussed above.

3.2. Steered Molecular Dynamics Simulation (SMD).

In order to analyze the behavior of a system toward a particular phenomenon which depends on a time scale much longer than that of a conventional MD simulation, SMD simulations can be employed.[25] An external force is used to cause the reactive movement in the simulated system and thus allows for the calculation of a path-dependent quantity. However, worth nothing is that the use of this pulling force perturbs the equilibrium of the system, thus precluding the calculation of thermodynamic quantities directly from the SMD trajectory without large errors.[44]

3.2.1. Energy Analysis of the Dissociation Process. The dissociation of the wild type UVR8 dimer and its mutants is a dynamic process. Upon commencement of the SMD simulation, the systems shift to a state of nonequilibrium. During the dissociation process, the change in interaction energy between the pulling regions was assessed for each system, as shown in Figure 3. Electrostatic and van der Waals (vdW) interactions

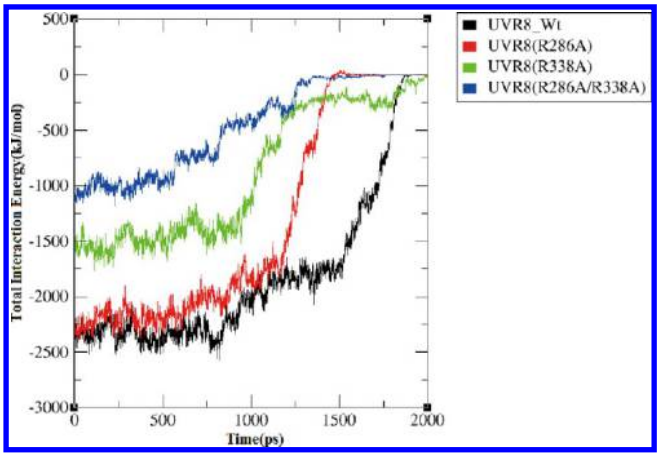

Figure 3. The total interaction energies at the interface of the UVR8 dimers of the wild type protein and its mutants during the SMD simulations.

predominantly contribute to the total interaction of each system, where the vdW interactions have a relatively smaller influence on the total energy. During the course of the pulling simulation, monomer A gradually shifts away from monomer B, and the total interaction energies are reduced (the energies become more positive).[45] At the starting point, the wild type UVR8 dimer has the strongest interface interaction energy, which is only slightly weaker in the R286A mutant system. In the interval between 1500 and 2000 ps, the energy curves quickly go to 0 for the wild type UVR8 dimer (shown in Figure 3). The same behavior occurs for the R286A mutant at about 1200–1500 ps, whereas in the R338A mutant system, the binding energy is rapidly weakened to 270 kJ/mol between 1000 and 2000 ps and then gradually reaches 0 at around 2000 ps. The weakest interaction energy is seen for the R286A/R338A double mutant system, which after only 500 ps of the SMD simulation starts to weaken even further, and where the interaction has disappeared after ~1200 ps.

By pulling the COM of monomer A away from monomer B of the UVR8 dimer, the force builds up until a dissociating point is reached, at which time the critical interactions are disrupted. The dissociation is a path-dependent process. Thus, the maximum force in each pulling simulation is not comparable to that of other simulations unless the dissociation pathway is very similar.[44]

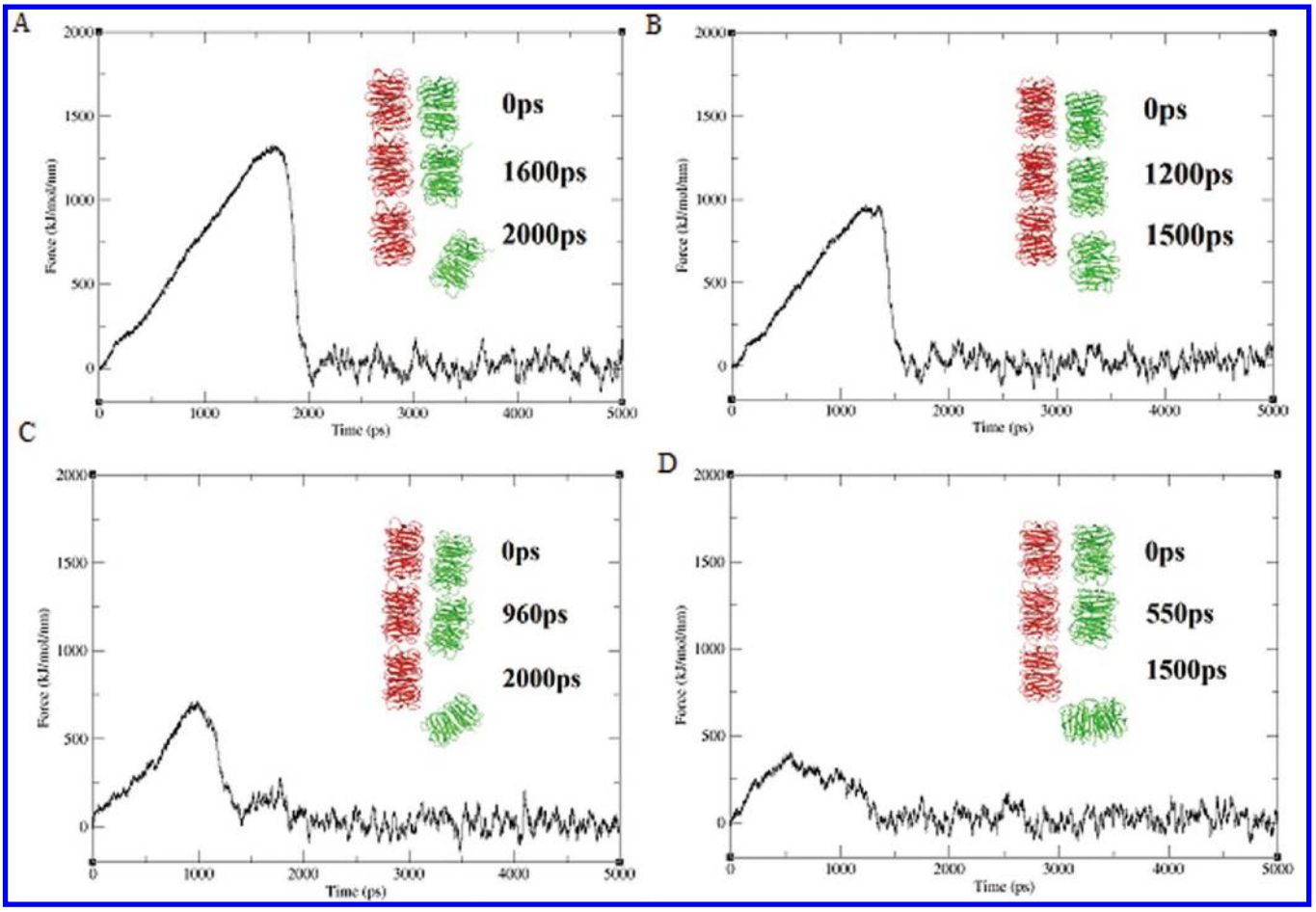

Figure 4. Dissociation pathways of the UVR8 wild type dimer and its mutants, with the corresponding plots of force vs time: (A) wild type, (B) R286A, (C) R338A, and (D) R286A/R338A.

In this work, the point of maximum force is 1326 kJ/mol/nm for the separation of the wild type UVR8 dimer and occurs at the simulation time ~1600 ps, as shown in Figure 4A. The maximum forces for the single mutants R286A and R338A and the double mutant R286A/R338A were obtained at simulation times 1400 ps, 950 ps, and 500 ps, respectively, and were reduced by 29%, 50%, and 70% compared to the wild type dimer (cf. Figure 4B–D). The forces drop to 0 with minor fluctuations after 2000 ps in the wild type UVR8 and the R338A mutant system, and around 1500 ps for the other mutants. This is in agreement with the timing of the vanishing interaction energies displayed in Figure 3. The structures of the dimer at the initial state, the dimer at the maximum force point, and the dissociated system are also shown for each oligomer in Figure 4.

3.2.2. Analysis of Salt Bridges during the Dissociation Process. Salt bridges are an abundant type of noncovalent interaction and are vital in stabilizing the UVR8 dimer structure. The key interface salt bridges are those formed between R146–E182, R200–D159, R286–D107/D96, R338–D44, and R354–E43/E53 in the wild type UVR8 dimer. The occurrence of these salt bridges during the dissociation processes is presented in Figure 5A. The cutoff radius of a salt bridge is defined as 0.35 nm between the heavy atoms (N and O). It can be seen that salt bridges from residues R146, R200, R286, R338, and R354 in monomers A and B formed with the corresponding carboxylate residues in monomers B and A, respectively, were with a few exceptions essentially stable during the SMD simulations until dissociation starts taking place in the interval 1600–1900 ps. No salt bridges from these residues remain after 1900 ps.

The salt bridges during the corresponding pulling process of the UVR8 mutant proteins are shown in Figure 5B–D. In the R286A mutant, the double hydrogen-bonded salt bridges between R286 and D107 are of course missing. Two relatively stable single hydrogen bonds between R338 and E43 in both monomers A and B are formed. In addition, residue R354 in monomer A forms a double hydrogen bond to E53 in monomer B until 1400 ps of the simulation. These are the longest lasting salt bridges found during the pulling process, as shown in Figure 5B, which indicates a strong interaction between these residues. After 1400 ps, no salt bridges prevail.

In the R338A mutant, the hydrogen bonds formed from residue R338 in the wild type are of course absent, and the double hydrogen-bonded salt bridges linking R286 with D107 are disrupted. However, the double hydrogen-bonded salt bridges joining R146 with E182 are conserved. A long-lived salt bridge between R200 in monomer B and D159 in monomer A was seen, which was present for a long time until the R338A mutant was completely dissociated. No salt bridges exist after 1900 ps, and the R200B–D159A salt bridge was the only one present in the interval 1200–1900 ps.

In the R286A/R338A double mutant, the salt bridges formed from residue R200 of both monomers are stable, and residue R354 in monomer B strongly hydrogen bonded to E43 in monomer A during the SMD simulations. No salt bridges were present after 1100 ps.

dx.doi.org/10.1021/ci4001822 | J. Chem. Inf. Model. 2013, 53, 1736–1746

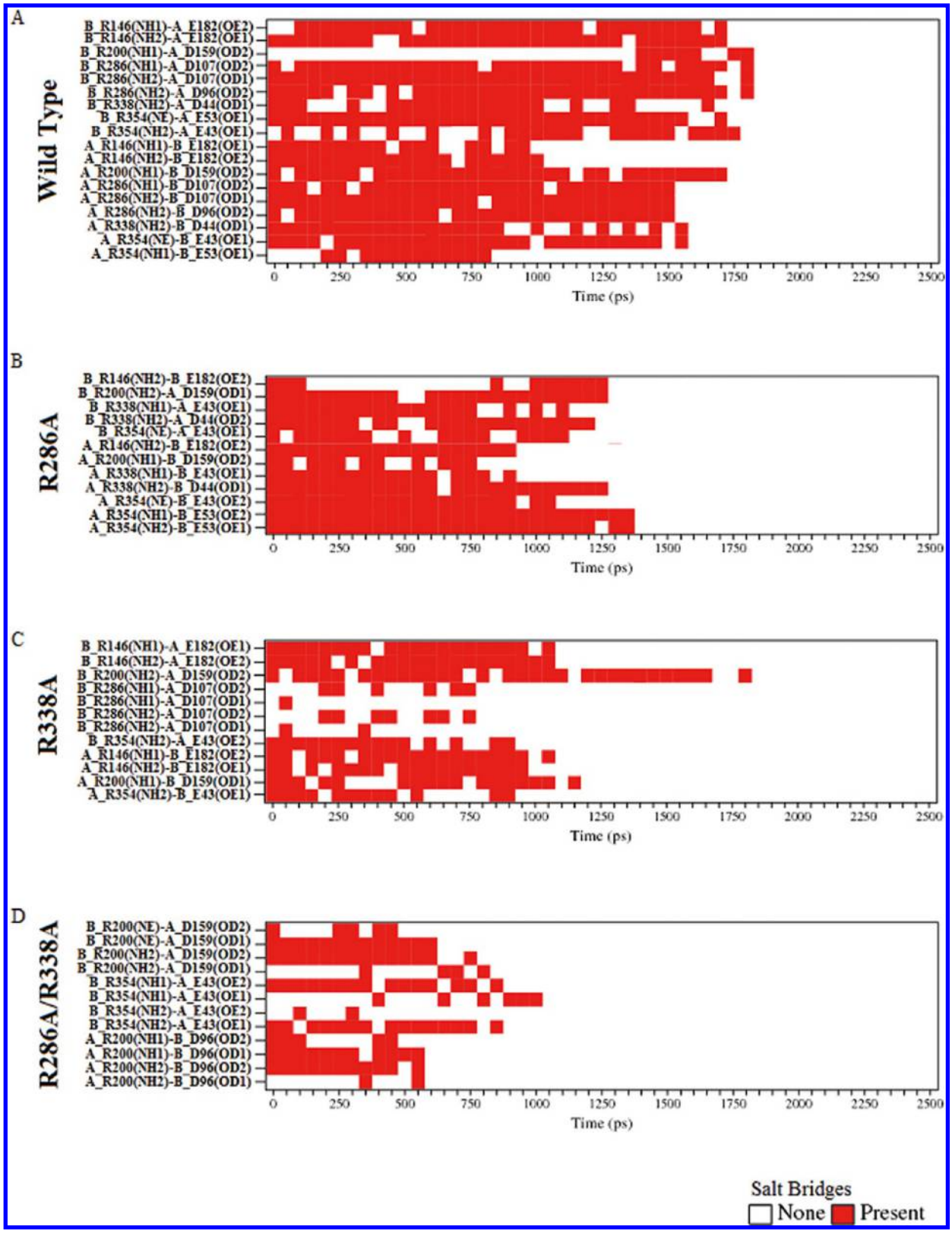

Figure 5. The presence of salt bridges between the different amino acid residues in monomers A and B, respectively. (A) Wild type UVR8; (B) R286A; (C) R338A; (D) R286A/R338A. Atom types NH1(2) and NE represent the nitrogen atoms from the primary and secondary amine groups in arginine, respectively, and atom types OD1(2) and OE1(2) represent the oxygen atoms from the carboxylate groups in aspartic acid and glutamic acid, respectively.

In order to determine the strengths of the interaction of the salt bridges between residues R146, R200, R286, R338, and R354 in monomer B and the entire monomer A during the steered simulations, the interaction energies were computed (Figure 6). In the wild type UVR8 dimer (Figure 6A), the interaction energies were stable except for R354 during the first 1800 ps, in

dx.doi.org/10.1021/ci4001822 | J. Chem. Inf. Model. 2013, 53, 1736−1746

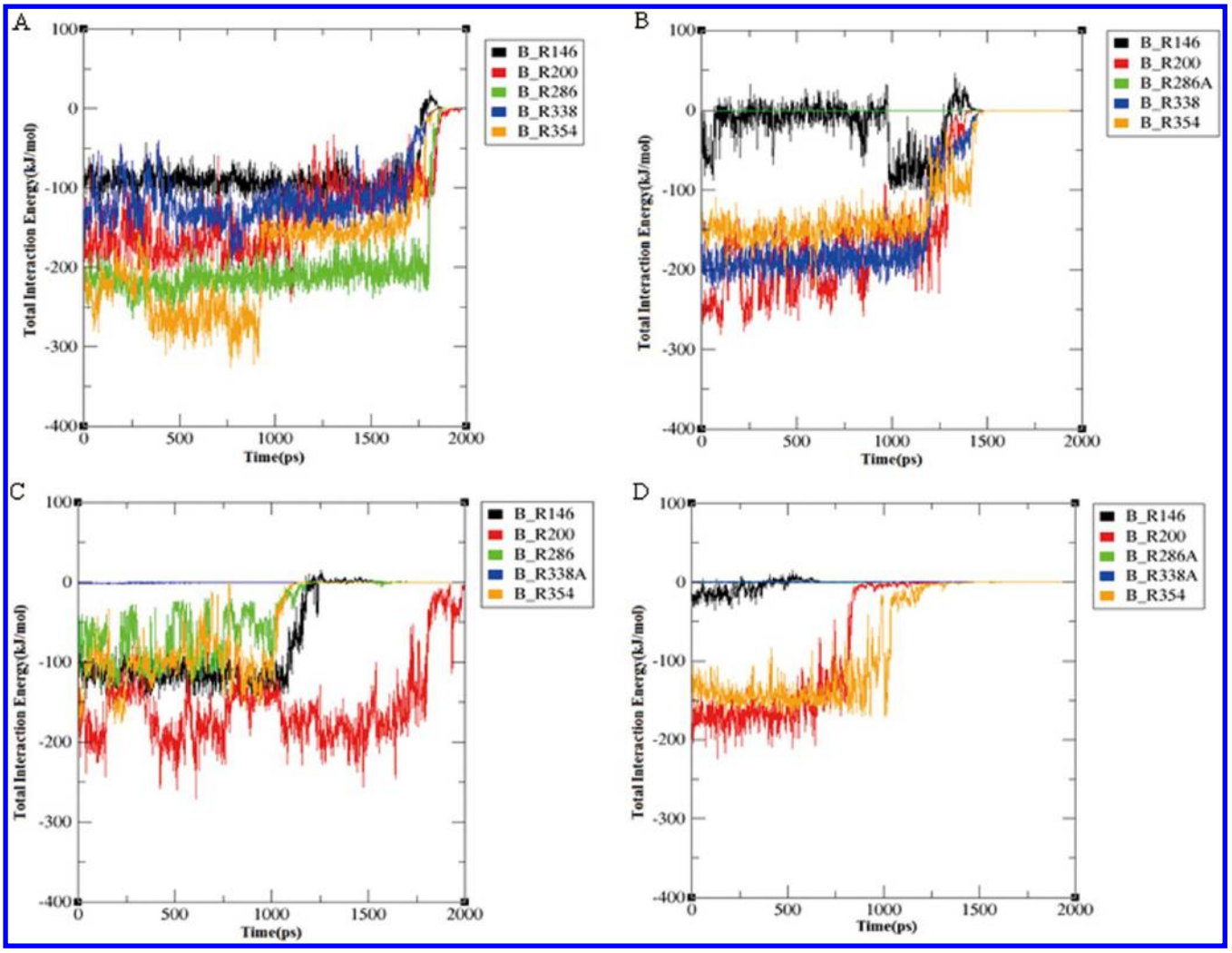

Figure 6. Time-dependence of the interaction energy for the amino acid residues of monomer B that are involved in interaction with monomer A during the SMD simulation. (A) Wild type UVR8 dimer, (B) R286A, (C) R338A, and (D) R286A/R338A.

agreement with the time of the maximum force shown in Figure 4A. The interaction energy for R146 was the weakest, around −90 kJ/mol, and for residues R286 and R338 was approximately −220 and −140 kJ/mol, respectively. The interaction energy for R200 was around −190 kJ/mol for the first 1300 ps, whereafter it gradually weakened to −100 kJ/mol during the following 400 ps. The interaction energy for R354 showed a large fluctuation with the strongest interaction energy during the first 900 ps and which then weakened to reach a stable value of −150 kJ/mol with minor fluctuation.

In the R286A mutant (Figure 6B), the interaction energy of R286A is of course equal to 0. For residue R146, the interaction energy first fluctuates around 0 until 900 ps, whereafter it obtains a value of −90 kJ/mol during the following 300 ps of simulation time. This is in agreement with the hydrogen bond between R146 in monomer B and E182 in monomer A that was disrupted and reformed (Figure 5B). The interaction energies of R338 and R354 were approximately −200 kJ/mol and −150 kJ/mol before 1200 ps, which was the time for the maximum force obtained during the pulling simulation shown in Figure 4B. From this point, steady reductions of the interaction energies were seen for residues R338 and R354. The interaction energy for R200 showed relatively large fluctuations around −200 kJ/mol during the simulation before dissociation.

In the R338A mutant (Figure 6C), the interaction energy was 0. Dramatic fluctuations in the interaction energies occurred for residues R200, R286, and R354, indicating repeated formation and loss of salt bridges for these residues. During the SMD simulation, all the interaction energies go to 0 at around 1000 ps, except for R200 for which the interaction energy reaches 0 after 2000 ps. This is also clearly seen in Figure 5C.

In the R286/R338 double mutant (Figure 6D), R146 had the weakest interaction energy, −30 kJ/mol at the starting point, which then rapidly decreased. R146 thus has a very small influence on the total interaction energy of the system. The interaction energy for R200 is strongest, around −170 kJ/mol, for the first 550 ps. It steadily weakened to −120 kJ/mol during the following 200 ps and quickly approached 0 around 850 ps. The behavior of the interaction energy for R354 was similar to that for R200; first the energy was approximately −150 kJ/mol for 800 ps; it then weakened to −100 kJ/mol with large fluctuations and finally rapidly disappeared at 1000 ps. It is intriguing that residue R200, to which there was no salt bridge formation found in the crystal structure of the UVR8 dimer,[10] had relatively strong interaction energies (−130 kJ/mol or more) in the wild type UVR8 dimer and its mutants in our present simulation study. This indicates that residue R200 may play a critical role in the rate of dissociation, although the static dimeric

dx.doi.org/10.1021/ci4001822 | J. Chem. Inf. Model. 2013, 53, 1736−1746

UVR8 structure as such was independent of this residue. We also emphasize the observation that the same amino acid residues of the two monomers interacted differently and that the dissociation path was nonsymmetric along the y axis.

3.3. Umbrella Sampling (US) Simulations. The force−time curves, generated in the COM pulling simulations, are sometimes insufficient to conclusively determine the stability of the wild type and mutant systems, especially for ΔG calculations.[44] Umbrella sampling simulations can thereby be used to determine ΔG of a particular event along a reaction coordinate ξ. In this work, the reaction coordinate is the COM separation along the y axis in Figure 1, for which umbrella sampling was performed by using 14−16 sampling windows with 40 ns of simulation time in each window. One-dimensional potential of mean force (PMF) curves were obtained for the wild type UVR8 dimer and its mutants (Figure 7) using the WHAM

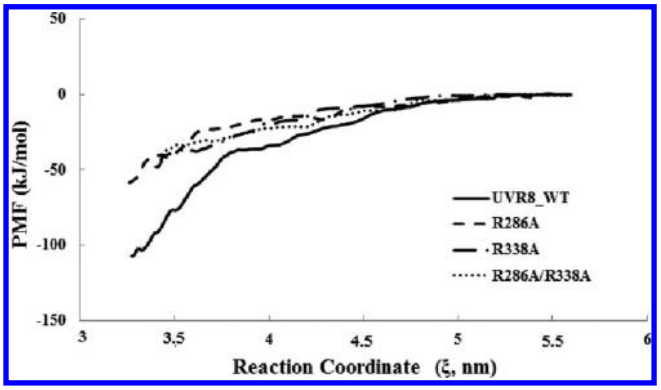

Figure 7. Potential of mean force (PMF) curves for dissociation of wild type (solid), R286A mutant (dashed), R338A mutant (dot-dashed), and R286A/R338A double mutant (dotted) UVR8 dimers.

method,[21−24] and the binding free energies were extracted (Table 2). Error analysis was conducted using a bootstrap method.[23,24]

Table 2. Binding Free Energies for the Wild-Type UVR8 Dimer and Its Mutants

system	ΔG_{Bind} (kJ/mol)[a]	$\Delta\Delta G_{Bind}$ (kJ/mol)
WT	−106.5	
R286A	−57.8	+48.7
R338A	−46.9	+59.6
R338A/R286A	−36.8	+69.7

[a]The error associated with energy minima is lower than ±2.1 kJ/mol for each system.

From the PMF curves, the energy minima occur at a COM distance of approximately 3.26 nm for the wild type UVR8 dimer, in agreement with the X-ray crystal structure obtained from the PDB (PDB code: 4DNW[10]), and approximately 3.27 nm, 3.37 nm, and 3.44 nm for the R286A, R338A, and R286A/R338A mutant systems, respectively. The distances between monomers A and B in the mutants R338A and R286A/E338A are longer than in the wild type and in the mutant R286A systems at their energy minima. This is especially true for the double mutant R286A/R338A. Taken together, this indicats that the single mutant R338A and the double mutant R286A/R338A lose a number of contacts at the interface between the monomers, in agreement with the results of the studies of the salt bridges presented in Figure 5, leading to instability of the dimer structure. However, this is not seen for the mutant R286A. The ΔG of dissociation is 106.5 kJ/mol for the wild type UVR8 dimer. The single mutations of R286 and R338 and the double mutation of R286/R338 to alanine reduce the binding energy ($\Delta\Delta G$) by 48.7 kJ/mol, 59.6 kJ/mol, and 69.7 kJ/mol, respectively. The reduced binding affinities are the result of a decreased number of native contacts, primarily salt bridges, which in turn results in destabilization of the dimeric structures.

4. CONCLUSION

Explicit solvent molecular dynamics (MD) simulations and steered molecular dynamics (SMD) simulations were employed to analyze interactions at the interface between the monomers of the wild type UVR8 dimer and several of its mutants, in order to demonstrate the key factors that are important for the stability of the dimer structure in UVR8. Interestingly, in the wild type UVR8 dimer and all its mutants studied here, residue R200, from which no salt bridges were seen either in the crystal structure[10] or after 100 ns MD simulations, has a relatively high interaction energy at the interface during the SMD simulations, especially in the R338A mutant. Although the dimeric X-ray structure is independent of residue R200, this residue may play a critical role for the rate of monomerization.

Umbrella sampling simulations using the weighted histogram analysis method (WHAM) were applied to calculate the binding free energies (ΔG) of the wild type UVR8 dimer and its mutants. In the dimers of the single mutant R338A and the double mutant R286A/R338A, the COM distances between monomers at the energy minima increased by 0.11 nm and 0.18 nm, respectively, whereas it only increased by 0.01 nm for the single mutant R286A. This indicated that at the equilibrium state, the loss of contact at the interface between monomers of single mutant R338A and double mutant R286A/R338A is substantial, but only slight for single mutant R286A. The solvent accessible surface area (SASA) analyses indicate that the dimeric interfaces of the mutants are more solvent-exposed than the wild type dimer. The average SASAs of the single mutants R286A and R338A and the double mutant R286A/R338A are increased by 4.05, 6.89, and 10.29 nm^2, respectively, compared to the wild type system, as obtained from the last 30 ns MD simulations. Furthermore, the binding energies ($\Delta\Delta G$) between the monomers of UVR8 mutants R286A, R338A, and R286A/R338A are reduced by 40%, 56%, and 65% relative to the wild type UVR8 dimer. The significant binding energy reduction for mutant R286A/R338A leads to complete monomerization.

Alanine substitutions with experimentally measured stabilizing effects correspond to reductions in binding energy of less than −3.76 kJ/mol. It has been suggested that a correctly identified hot spot residue should show a change in binding free energy by more than 4.18 kJ/mol, upon mutation to alanine.[46] We thus conclude that both residues R338 and R286 are hot spot residues in stabilizing the dimeric structure of UVR8. The binding energy reductions for single mutants R338A are relatively speaking larger than for R286A, which indicates that R338 appears more crucial than R286 for the dimeric stability. Considering that the COM distances between the monomers only increase by 0.01 nm at the energy minimum point, for single mutant R286A compared to the wild type, we furthermore conclude that both the monomeric and the dimeric UVR8 structures thus may exist for single mutant R286A, although it has larger than 4.18 kJ/mol binding free energy reduction compared to the wild type system.

dx.doi.org/10.1021/ci4001822 | J. Chem. Inf. Model. 2013, 53, 1736−1746

This explains the diverging experimental results obtained in previous studies.[7,10]

■ ASSOCIATED CONTENT

Supporting Information

The resulting histograms for umbrella sampling simulations are shown in Figure S1; the ΔG_{Bind} vs simulation time in Figure S2; atom types labeled for N, O, and C atoms in arginine, aspartic acid, and glutamic acid in Figure S3; the structures of UVR8 mutants at a 100 ns snapshot in Figure S4; and Cα RMSDs of the wild type UVR8 dimer and mutants during the MD simulations in Figure S5. The information is available free of charge via the Internet at http://pubs.acs.org

■ AUTHOR INFORMATION

Corresponding Author

*E-mail: leif.eriksson@chem.gu.se.

Notes

The authors declare no competing financial interest.

■ ACKNOWLEDGMENTS

University of Gothenburg is gratefully acknowledged for financial support (L.A.E), as is the Faculty of Business, Science and Technology at Örebro University (Å.S.). Grants of computing time at the Irish Center for High-End Computing (ICHEC) and the C3SE Supercomputing Center at Chalmers (Göteborg) are gratefully acknowledged.

■ REFERENCES

(1) Bornman, J. F. Target sites of UV-B radiation in photosynthesis of higher plants. *J. Photochem. Photobiol., B* **1989**, *4*, 145−158.

(2) Strid, Å.; Chow, W. S.; Anderson, J. M. UV-B damage and protection at the molecular level in plants. *Photosynth. Res.* **1994**, *39*, 475−489.

(3) Hideg, É.; Jansen, M. A. K.; Strid, Å. UV-B exposure, ROS and stress: inseparable companions or loosely linked associates? *Trends Plant Sci.* **2012**, *18*, 107−115.

(4) Wu, M.; Xu, Q.; Strid, Å.; Martell, J. M.; Eriksson, L. A. Theoretical study of pyridoxine (vitamin B6) photolysis. *J. Phys. Chem. A* **2011**, *115*, 13556−13563.

(5) Jansen, M. A. K.; Coffey, A. M.; Prinsen, E. UV-B induced morphogenesis: Four players or a quartet? *Plant Signaling Behav.* **2012**, *7*, 1185−1187.

(6) Brown, B. A.; Cloix, C.; Jiang, G. H.; Kaiserli, E.; Herzyk, P.; Kliebenstein, D. J.; Jenkins, G. I. A UV-B-specific signaling component orchestrates plant UV protection. *Proc. Natl. Acad. Sci. U. S. A.* **2005**, *102*, 18225−18230.

(7) Christie, J. M.; Arvai, A. S.; Baxter, K. J.; Heilmann, M.; Pratt, A. J.; O'Hara, A.; Kelly, S. M.; Hothorn, M.; Smith, B. O.; Hitomi, K.; Jenkins, G. I.; Getzoff, E. D. Plant UVR8 photoreceptor senses UV-B by tryptophan-mediated disruption of cross-dimer salt bridges. *Science* **2012**, *335*, 1492−1496.

(8) Heijde, M.; Ulm, R. UV-B photoreceptor-mediated signalling in plants. *Trends Plant Sci.* **2012**, *17*, 230−237.

(9) Jenkins, G. I. Signal transduction in responses to UV-B radiation. *Annu. Rev. Plant Biol.* **2009**, *60*, 407−431.

(10) Wu, D.; Hu, Q.; Yan, Z.; Chen, W.; Yan, C.; Huang, X.; Zhang, J.; Yang, P.; Deng, H.; Wang, J.; Deng, X.; Shi, Y. Structural basis of ultraviolet-B perception by UVR8. *Nature* **2012**, *484*, 214−219.

(11) Brown, B. A.; Jenkins, G. I. UV-B signaling pathways with different fluence-rate response profiles are distinguished in mature Arabidopsis leaf tissue by requirement for UVR8, HY5, and HYH. *Plant Physiol.* **2008**, *146*, 576−588.

(12) Favory, J. J.; Stec, A.; Gruber, H.; Rizzini, L.; Oravecz, A.; Funk, M.; Albert, A.; Cloix, C.; Jenkins, G. I.; Oakeley, E. J.; Seidlitz, H. K.; Nagy, F.; Ulm, R. Interaction of COP1 and UVR8 regulates UV-B-induced photomorphogenesis and stress acclimation in Arabidopsis. *EMBO J.* **2009**, *28*, 591−601.

(13) Kaiserli, E.; Jenkins, G. I. UV-B promotes rapid nuclear translocation of the Arabidopsis UV-B specific signaling component UVR8 and activates its function in the nucleus. *Plant Cell* **2007**, *19*, 2662−2673.

(14) Rizzini, L.; Favory, J. J.; Cloix, C.; Faggionato, D.; O'Hara, A.; Kaiserli, E.; Baumeister, R.; Schäfer, E.; Nagy, F.; Jenkins, G. I.; Ulm, R. Perception of UV-B by the Arabidopsis UVR8 protein. *Science* **2011**, *332*, 103−106.

(15) Brown, B. A.; Headland, L. R.; Jenkins, G. I. UV-B action spectrum for UVR8-mediated HY5 transcript accumulation in *Arabidopsis*. *Photochem. Photobiol.* **2009**, *85*, 1147−1155.

(16) Cloix, C.; Kaiserli, E.; Heilmann, M.; Baxter, K. J.; Brown, B. A.; O'Hara, A.; Smith, B. O.; Christie, J. M.; Jenkins, G. I. C-terminal region of the UV-B photoreceptor UVR8 initiates singaling through interaction with the COP1 protein. *Proc. Natl. Acad. Sci. U. S. A.* **2012**, *109*, 16366−16370.

(17) Yi, C.; Deng, X. W. COP1 - from plant photomorphogenesis to mammalian tumorigenesis. *Trends Cell Biol.* **2005**, *15*, 618−625.

(18) Oravecz, A.; Baumann, A.; Máté, Z.; Brzezinska, A.; Molinier, J.; Oakeley, E. J.; Adám, E.; Schäfer, E.; Nagy, F.; Ulm, R. CONSTITUTIVELY PHOTOMORPHOGENIC1 is required for the UV-B response in Arabidopsis. *Plant Cell* **2006**, *18*, 1975−1990.

(19) Wu, M.; Grahn, E.; Eriksson, L. A.; Strid, Å. Computational evidence for the role of *Arabidopsis thaliana* UVR8 as UV-B photoreceptor and identification of its chromophore amino acids. *J. Chem. Inf. Model.* **2011**, *51*, 1287−1285.

(20) O'Hara, A.; Jenkins, G. I. In vivo funtion of tryptophans in the *Arabidopsis* UV-B photoreceptor UVR8. *Plant Cell* **2012**, *24*, 3755−3766.

(21) Jarzynski, C. Nonequilibrium equality for free energy differences. *Phys. Rev. Lett.* **1997**, *78*, 2890−2693.

(22) Kumar, S.; Rosenberg, J. M.; Bouzida, D.; Swendsen, R. H.; Kollman, P. A. The weighted histogram analysus method for free-energy calculations on biomolecules. I. The method. *J. Comput. Chem.* **1992**, *13*, 1011−1021.

(23) Hub, J. S.; de Groot, B. L.; van der Spoel, D. g_wham-A free weighted histogram analysis implementation including rohust error and autocorrelation estimates. *J. Chem. Theory Comput.* **2010**, *6*, 3713−3720.

(24) Hub, J. S.; de Groot, B. L. Does CO2 permeate through Aquaporin-1? *Biophys. J.* **2006**, *91*, 842−848.

(25) Izrailev, S.; Stepaniants, S.; Isralewitz, B.; Kosztin, D.; Lu, H.; Molnar, F.; Wriggers, W.; Schulten, K. Steered Molecular Dynamics. In *Computational Molecular Dynamics: Challenges, Methods, Ideas*, 1st ed.; Deuflhard, P., Hermans, J., Leimkuhler, B., Mark, A. E., Reich, S., Skeel, R. D., Eds.; Springer-Verlag: Berlin, 1998; Vol. *4*, pp 39−65.

(26) Torrie, G. N.; Valleau, J. P. Nonphysical sampling distributions in Monte Carlo free-energy estimation: Umbrella sampling. *J. Comput. Phys.* **1977**, *23*, 187−199.

(27) Torrie, G. N.; Valleau, J. P. Monte Carlo free energy estimates using non-Boltzmann sampling:Application to the sub-critical Lennard-Jones fluid. *Chem. Phys. Lett.* **1974**, *28*, 578−581.

(28) Patey, G. N.; Valleau, J. P. The free energy of spheres with dipoles: Monte Carlo with multistage sampling. *Chem. Phys. Lett.* **1973**, *21*, 297−300.

(29) Woo, H. J.; Roux, B. Calculation of absolute protein-ligand binding free energy from computer simulations. *Proc. Natl. Acad. Sci. U. S. A.* **2005**, *102*, 6825−6830.

(30) Doudou, S.; Burton, N. A.; Henchman, R. H. Standard free energy of binding from a one-dimensional potential of mean force. *J. Chem. Theory Comput.* **2009**, *5*, 909−918.

(31) Gumart, J. C.; Roux, B.; Chipot, C. Standard binding free energies from computer simulations: What is the best strategy? *J. Chem. Theory Comput.* **2013**, *9*, 794−802.

(32) *Molecular Operating Enviroment*, version 2011.10; Chemical Computing Group Inc.: Montreal, Quebec, Canada, 2011.

(33) Hess, B.; Kutzner, C.; Van der Spoel, D.; Lindahl, E. Gromacs 4: Algorithms for highly efficient, load-balanced, and scalable molecular simulation. *J. Chem. Theory Comput.* **2008**, *4*, 435−447.
(34) GROMACS. http://www.gromacs.org/ (accessed date May 8, 2013).
(35) Duan, Y.; Wu, C.; Chowdhury, S.; Lee, M. C.; Xiong, G.; Zhang, W.; Yang, R.; Cieplak, P.; Luo, R.; Lee, T.; Caldwell, J.; Wang, J.; Kollman, P. A point-charge force field for molecular mechanics simulations of proteins based on condensed-phase quantum mechanical calculations. *J. Chem. Theory Comput.* **2003**, *24*, 1999−2012.
(36) Darden, T.; York, D.; Pedersen, L. Particle mesh Ewald: An N-log(N) method for Ewald sums in large systems. *J. Chem. Phys.* **1993**, *98*, 10089−10092.
(37) Essmann, U.; Perera, L.; Berkowitz, M. L.; Darden, T.; Lee, H.; Pedersen, L. G. A smooth particle mesh Ewald method. *J. Chem. Phys.* **1995**, *103*, 8577−8593.
(38) Berendsen, H. J. C.; Postma, J. P. M.; van Gunsteren, W. F.; DiNola, A.; Haak, J. R. Molecular dynamics with coupling to an external bath. *J. Chem. Phys.* **1984**, *81*, 3684−3690.
(39) Hoover, W. G. Canonical dynamics: Equilibrium phase-space distributions. *Phys. Rev. A* **1985**, *31*, 1695−1697.
(40) Nosé, S. J. A unified formulation of the constant temperature molecular dynamics methods. *J. Chem. Phys.* **1984**, *81*, 511−519.
(41) Nosé, S.; Klein, M. L. A study of solid and liquid crbon tetrafluoride using the constant pressure molecular dynamics technique. *J. Chem. Phys.* **1983**, *78*, 6928−6939.
(42) Parrinello, M.; Rahman, A. Polymorphic transitions in single crystals: A new molecular dynamics method. *J. Appl. Phys.* **1981**, *52*, 7182−7190.
(43) YASARA. http://www.yasara.org (accessed date May 8, 2013).
(44) Lemkul, J. A.; Bevan, D. R. Assessing the stability of alzheimer's amyloid protofibrils using molecular dynmaics. *J. Phys. Chem. B* **2009**, *114*, 1652−1660.
(45) Shen, M.; Guan, J.; Xu, L.; Yu, Y.; He, J.; Jones, G. W.; Song, Y. Steered molecular dynamics simulations on the binding of the appendant structure and helix-β2 in domain-swapped human cystatin C dimer. *J. Biomol. Struct. Dyn.* **2012**, *30*, 652−661.
(46) Kortemme, T.; Baker, D. A simple physical model for binding energy hot spots in protein-protein complexes. *Proc. Natl. Acad. Sci. U. S. A.* **2002**, *99*, 14116−14121.